36(16): 3515–3531, 2003 – which should be cited to refer to this work.

Electron spectra for associative detachment in low-energy collisions of Cl^- and Br^- with H and D†

S Živanov[1], M Čížek[1,2], J Horáček[1,2] and M Allan[1]

[1] Department of Chemistry, University of Fribourg, chemin du Musée 9, CH-1700 Fribourg, Switzerland
[2] Institute of Theoretical Physics, Faculty of Mathematics and Physics, Charles University Prague, V Holešovičkách 2, 1800 Praha 8, Czech Republic

Abstract

Energy spectra of electrons detached in collisions of Cl^- and Br^- with atomic hydrogen and deuterium have been measured for laboratory frame ion energies between 0.2 and 8.0 eV. Their shapes agree very well with the predictions of nonlocal resonance theory. Both types of structure predicted by the theory are observed. They are the 'v steps', at ro-vibrational thresholds, and the 'S steps', which are a consequence of interchannel coupling, which raises the cross section when a higher vibrational channel closes. They exhibit the behaviour predicted by theory both when the collision energy is varied and upon isotope substitution. The 'v steps' move to higher electron energies with higher collision energy and when hydrogen is substituted by deuterium, reflecting the higher maximum energy available to the electron. The positions of the S steps do not depend on collision energy, and are essentially equal to differences of vibrational energies of the product molecules HCl, DCl, HBr and DBr. The relative cross sections for formation of low vibrational levels (i.e., emission of fast electrons) are smaller in the deuterated compounds, reflecting the slower motion of D compared to H and consequently preferred detachment at high internuclear separations.

1. Introduction

Associative electron detachment is an important plasma process. Here we are concerned with the collisions of the halogen anions Cl^- and Br^- with atomic hydrogen,

$$H + X^-(E_{rel}) \longrightarrow HX(v, J) + e^-(\varepsilon),$$

where H designates both the ^1H and ^2H isotopes, X is the halogen, E_{rel} is the centre-of-mass (CMS) collision energy, v and J the vibrational and rotational quanta of the product molecule and ε the energy of the detached electron.

† Dedicated to Professor Hartmut Hotop, on the occasion of his 60th birthday.

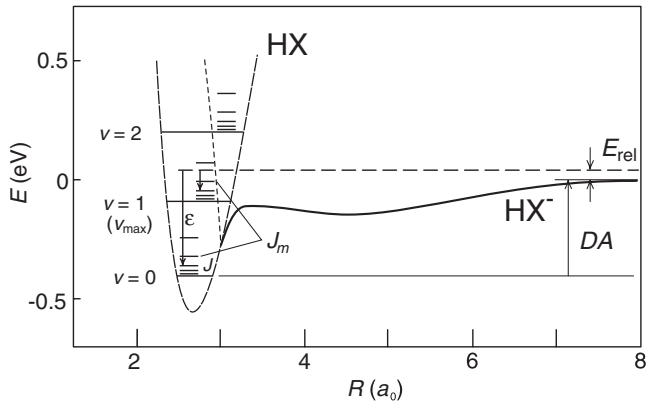

Figure 1. Schematic diagram of potential curves relevant for associative detachment, corresponding approximately to the $H + Br^-$ case. E_{rel} is the CMS collision energy and DA the threshold energy for dissociative attachment. Two competing transitions into two different final vibrational but the same final rotational levels are indicated by vertical arrows. The separation of the rotational levels is shown exaggerated for clarity.

The process is illustrated schematically in figure 1. The collision partners approach on the negative ion potential curve with a given angular momentum, J, associated, in classical terms, with the impact parameter, b. At a given internuclear distance, the negative ion and the neutral molecule potential curves cross, and the negative ion becomes a resonance which can be described with various degrees of approximation as detailed further below. Note that each collision is characterized by a given J and the detachment is consequently characterized by competition of various final vibrational states v but only one given value of J, as indicated by vertical arrows. The collision is dominated by an s wave in hydrogen halides, the departing electron does not carry angular momentum and the initial orbital angular momentum agrees with the J of HX in the final state. The highest vibrational levels accessible at low collision energies range from $v_{max} = 1$ for HBr (as shown in the figure) to $v_{max} = 3$ in DCl. The dominance of an s wave and consequently the absence of a rotational barrier for the departing electron make the autodetachment rate high. The detachment occurs early in the collision, at large internuclear distances, preferring the highest available v. The energies ε of the departing electrons carry information about the final ro-vibrational state, and the product state distribution can consequently be obtained experimentally from electron spectra.

Čížek *et al* (2001b) have shown that the theoretical description of the details of the associative detachment process in hydrogen–halogen anion collisions is intricate because of the necessity of using a theoretical model which correctly describes threshold processes. Only such a theory takes into account coupling between the various v channels, which plays a decisive role in the present system where the s wave dominates. An early approach, which described qualitatively correctly the threshold features in resonance collisions and the interchannel coupling, is the zero-range-potential approximation (ZRP), used for calculations of F^-/H and Cl^-/H associative detachment by Gauyacq (1982, 1987). ZRP is a limiting case of the R-matrix theory (Schneider *et al* 1979, Schramm *et al* 1999).

The local complex potential (LCP) theory, often used to describe resonances, does not have this capacity. The more general nonlocal resonance theory (Domcke 1991) overcomes the shortcoming of the LCP, and has been shown to correctly describe all observed threshold features in low-energy electron collisions with hydrogen halides (Čížek *et al* 2001a). Čížek *et al* (2001b) applied the nonlocal theory to associative detachment, and obtained a prediction

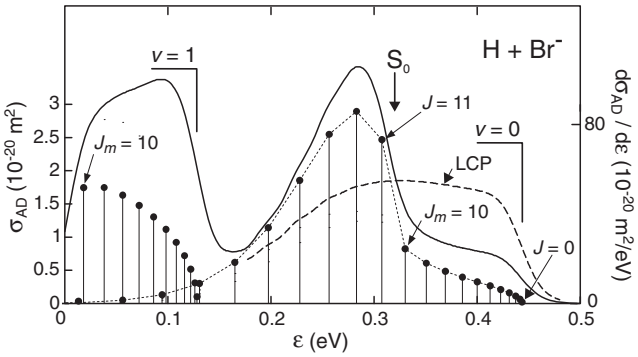

Figure 2. Diagram of the cross sections for associative detachment into individual ro-vibrational final states of HBr ($\sigma_{\rm AD}$, vertical bars with dots) and the resulting spectrum of the detached electrons ($\mathrm{d}\sigma_{\rm AD}/\mathrm{d}\varepsilon$, solid curve), convoluted by a simulated instrumental resolution of 30 meV. The interchannel coupling is manifested by the rise of the cross section in the $v = 0$ channel for $J > J_{\rm m}$, leading to the S_0 step in the spectrum. This step is missing in the spectrum of the detached electrons predicted by the LCP model, indicated by a dashed curve. The CMS collision energy is 50 meV (adapted from Čížek *et al* (2001b)).

of the spectra of the detached electrons differing dramatically from that of the LCP theory. The difference is illustrated in figure 2, which shows the cross sections for the individual final ro-vibrational states as they appear in the spectrum of the detached electrons.

A naive expectation of the J dependence of the cross sections leads to signals initially increasing with increasing J (i.e., with decreasing electron energy ε), causing steps in the signals at the ro-vibrational thresholds (indicated by vertical bars and the values of the corresponding v in figure 2). We shall call these structures the 'v steps'. The cross section will then eventually decrease as (in classical terms) the impact parameter, b, increases beyond the distance of curve crossing. This expectation is born out by the LCP theory. The nonlocal theory indicates, however, that the $v = 0$ and 1 channels are coupled and the $v = 0$ cross section rises sharply above $J = 10$ when the $v = 1$ channel closes, giving rise to the S_0 step (Čížek *et al* 2001a). Generally, the closing of the highest accessible vibrational channel, $v_{\rm max}$, for rotational angular momenta, J, beyond the maximum value, $J_{\rm m}$, causes steplike onsets (which we shall label as S_v) in the rotational distributions for the lower vibrational levels ($v < v_{\rm max}$) at $J = J_{\rm m}$. They are located at the energy $\varepsilon(S_v) = G(v_{\rm max}) - G(v) + (B_{v_{\rm max}} - B_v)J_{\rm m}(J_{\rm m}+1)$. Typically, the rotational energy difference is small compared to the vibrational term difference, i.e., the onset energy for the step S_v is simply located at the energy difference $G(v_{\rm max}) - G(v)$, which is independent of collision energy. This is in contrast to the v steps, whose energy depends on $E_{\rm rel}$. The steps S_v are a manifestation of channel interaction and as such are closely related to Wigner cusps in dissociative attachment of electrons to hydrogen halides discovered by Abouaf and Teillet-Billy (1977), except that here we observe the structures in the J dependence instead of the energy dependence of the cross section.

Early experimental studies of associative detachment by Howard *et al* (1974) measured the rate coefficients. Huels *et al* (1994) determined the total cross sections for associative detachment in $H + X^-$ collisions as a function of collision energy in a crossed beam experiment, and found them, in agreement with a classical model calculation, to increase rapidly with decreasing collision energy. The total cross sections do not represent a sensitive probe of the mechanism, however, because they do not provide information on the distribution of the final vibrational and rotational states of the product molecules. Valuable information on the relative

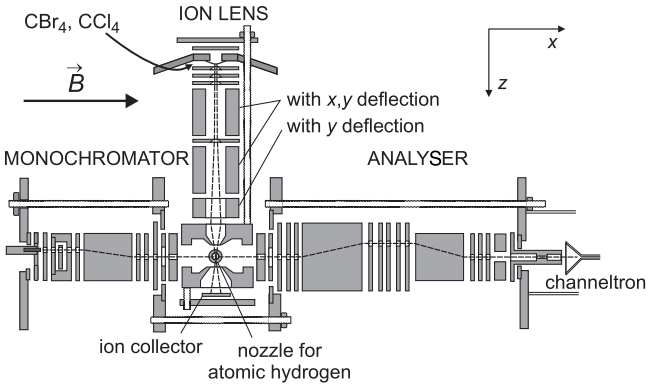

Figure 3. Schematic diagram of the instrument. Electron and ion beams are indicated by dashed lines. The monochromator is used only for diagnostic purposes and not while recording associative detachment spectra.

(rotationally summed) populations of the final vibrational levels (e.g. in HF and HCl) was gained by infrared emission spectroscopy in a flowing afterglow by Zwier *et al* (1980) and by Smith and Leone (1983). Detailed information on the final vibrational and rotational state population is provided by the energy spectra of the detached electrons, reported by Živanov *et al* (2002). The results fully confirmed the presence of the S_v steps.

The present study extends the study of Živanov *et al* (2002). We present calculated and measured spectra of detached electrons for various collision energies to verify the behaviour of the two types of structure. We further study the effect of isotope substitution by measuring collisions with deuterium atoms.

2. Methods

2.1. Experiment

The experimental set-up has been briefly described by Živanov *et al* (2002). Its design presented several challenges. Both collision partners are reactive and have to be prepared *in situ* in sufficient densities. The halogen anions must be decelerated to sufficiently low energies. Measurement of the spectra of detached electrons requires an analyser with high sensitivity and a controlled response function down to very low energies.

Our instrument, shown schematically in figure 3, is based on the magnetically collimated electron spectrometer described by Allan (1989) and by Asmis and Allan (1997). It uses the trochoidal electron energy analysers of Stamatović and Schulz (1968) and provides the required high detection efficiency for slow electrons and controlled response function down to about 50 meV. The collision region has been modified for crossed-beam operation, and a halogen anion beam source as well as a microwave-discharge based source of atomic hydrogen have been added.

The Cl^- and Br^- ions are produced from CCl_4 and CBr_4 in the vicinity of a standard thoria coated iridium ribbon filament, in an arrangement similar to that used by Allan (1982) for the preparation of O^-. The mechanism of formation is presumably dissociative attachment of thermal electrons present in large number in the vicinity of the hot filament, although surface reactions cannot be excluded. The ions are formed into a beam and transported into the collision region by a three-cylinder lens designed with the help of the CPO-3D program of Read and

Bowring. Ions are separated from electrons emanating from the filament by the magnetic field of the trochoidal spectrometer which is perpendicular to the propagation of the anions. An electron attenuation factor in excess of 10^4 was attained. The much weaker deflection of ions was offset by two pairs of 'x–y' deflectors and one additional 'y' deflection in the ion lens. The ion source does not provide mass selection, except the separation of ions and electrons. We therefore duplicated the ion source in a separate experiment where a quadrupole mass spectrometer allowed mass analysis of the ion beam, and verified that only Cl^- and Br^- anions are formed from CCl_4 and CBr_4, respectively, under these conditions.

The nominal laboratory frame ion energy is given by the voltage difference between the filament and the collision region. Differences in contact potentials between the filament and the molybdenum parts around the collision region could make the true ion energy different from this voltage difference, however. In addition, both the ion energy and the energy spread could be significantly affected if ions were produced in the extraction field region between the filament and the anode. We derived indication of both the ion energies and the energy spread from the retardation curves shown in figure 4. They were obtained by recording ion current as a function of the voltage on the ion collector (see figure 3). They were recorded with the atomic hydrogen source turned on—the curves measured in the absence of atomic hydrogen were shifted by about 0.5 eV to lower retarding potentials. The ion trajectory simulations with the CPO-3D program indicate that the ion current is lost not exactly when the ions are decelerated to zero energy, but about 50 meV before, due to defocusing of the ion beam. The inflection points of the retardation curves in figure 4 are slightly below the ion accelerating voltage difference (i.e., the nominal ion energy), indicating that the nominal ion energy scale is correct within about ± 0.3 eV. The energy spread derived from the retardation curves is about 0.4 eV. Both findings indicate that the Cl^- and Br^- anions are formed at or very near the filament surface and their final energies and energy spread are not significantly affected by the draw-out field. The accuracy of the nominal ion energy scale and the ion energy spread are adequate for our experiment because the laboratory frame energies are greatly compressed in the CMS frame (Čížek *et al* 2001b). The ion currents of the present experiment have been improved with respect to the previous experiment of Živanov *et al* (2002) by better sealing the volume around the ion producing filament and thus increasing the local CCl_4 or CBr_4 pressure.

Our microwave based source of atomic hydrogen follows the design of Paolini and Khakoo (1998). The discharge takes place in an 8 mm diameter air cooled fused silica tube with a 1 mm diameter constriction after the discharge that provides a build-up of the gas pressure in the discharge region and prevents spread of the discharge into the instrument. The discharged hydrogen is transported to the collision region by a $\sim$20 cm long PTFE tube and a fused silica tube with a 1 mm diameter nozzle, painted on the outside with colloidal graphite. The discharge tubes were immersed in ortho-phosphoric acid overnight, washed with deionized water and dried at 125 °C before installation.

The electron energy loss mode of the spectrometer is used to monitor and optimize the density of H atoms prior to the associative detachment measurements. A typical energy loss spectrum is shown in figure 5. Small amounts of water vapour added to the discharge were found to increase the yield of atomic hydrogen as reported by Spence and Inokuti (1974) and Burrow (2001). A weak signal appears in the energy loss spectra to the left of the $n = 2$ line of atomic hydrogen in the presence of water. We verified that the water vapour makes no measurable contribution to the associative detachment spectra. The residual molecular hydrogen also does not contribute to the associative detachment signal at the relevant collision energies. Part of the residual H_2 signal in the energy loss spectrum is due to background gas in the main vacuum chamber, with H atoms recombined on its walls. The energy loss experiment probes the background gas along a path much longer than the region where the

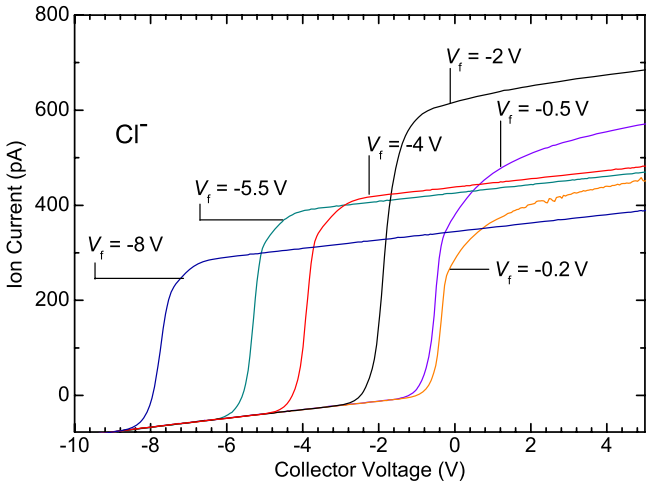

Figure 4. Cl^- retardation curves for various potentials of the ion forming filament V_f, measured with respect to the electrodes around the collision region. The nominal ion energy E_{Cl^-} is equal to $-V_f$.

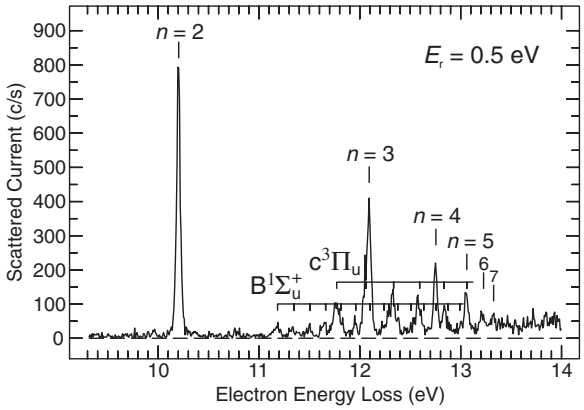

Figure 5. Energy-loss spectrum of discharged hydrogen, recorded at a constant residual energy of 0.5 eV. The transitions of atomic hydrogen as well as two transitions of the residual molecular hydrogen are marked.

ion and the discharged hydrogen beams cross. Figure 5 thus gives a somewhat pessimistic view of the fraction of hydrogen which has been dissociated. We estimated the ratio of atomic and molecular hydrogen densities in the target region to be $N_H/N_{H_2} \approx 1.4$, using the relative areas under the $n = 2$ peak of H and the $v = 2$ band of the B $^1\Sigma_u^+$ state of H_2 in the energy loss spectra. The relevant differential cross sections were taken from a CCC calculation of Bray (2001) for H (sum of the 2 ^{2}S and 2 ^{2}P states, average of 0° and 180°) and from the measurements of Weingartshofer *et al* (1970) for H_2 (average of 0° and 180° cross sections, obtained by extrapolation of their 10°–120° data).

The electric field in the collision region is defined by two flat electrodes with conically shaped entrance and exit apertures for the ions. The potentials of these electrodes can be varied independently. A small voltage difference between them is generally required to guide the electrons from associative detachment into the entrance aperture of the analyser, that is to

compensate for stray electric field and the fact that, because of axial magnetic field, the anions enter the collision region slightly off axis.

The standard way of calibrating the energy scales of the trochoidal spectrometer would require that the discharge is turned off and hydrogen is replaced by nitrogen. The discharged hydrogen causes large drifts of the contact potentials of the electrodes, however, and the energy scales had to be calibrated with the hydrogen discharge on, in the absence of N_2. We therefore calibrated the onset of the electron signal on the position of narrow resonant structures in the differential cross section for the excitation of the $n = 2$ transitions of atomic hydrogen, which we know from high-level convergent close coupling (CCC) calculations of Bray (2001). The individual AD spectra are then calibrated on the onset of the electron signal. The scale is reliable to ± 30 meV.

The width of the energy-loss peak in figure 5 is 45 meV, indicating an analyser resolution of $\sim$32 meV. The resolution varied somewhat from run to run, however, and could be slightly worse in some of the spectra shown here. The spectra have been corrected for the response function of the analyser, based on our previous experiments with helium and on a numerical treatment of electron trajectories (Asmis and Allan 1997). The correction procedure is reliable to within about $\pm 30\%$ at energies above 100 meV, less reliable below. Our experiment measures relative cross sections. We compare the shapes of the experimental and the theoretical curves, but not the absolute magnitudes, which are normalized arbitrarily.

2.2. CMS collision velocity distribution

The knowledge of the CMS collision velocity distribution $f(v_{\rm rel})$ is important for the comparison of the present experiments with the theory. The thermal velocity spread of the hydrogen (or deuterium) atoms makes a dominant contribution to the width of this distribution, in view of their low mass and the low ion kinetic energies used in this work. Čížek *et al* (2001b) used a numerical integration of the CMS energies over the applicable ranges of collision parameters such as collision energies and collision angles to determine $f(v_{\rm rel})$. The mean collision angle is 90° in the present experiment, in contrast to the 60° assumed by Čížek *et al* (2001b). The spread of collision angles is harder to obtain. The angular spread of the hydrogen atoms leaving the essentially effusive nozzle is large, but the instrument probes only a small volume in the atomic beam. The size of the effective collision volume in the y and z directions (figure 3) is given by the diameter of the analyser acceptance cylinder, constricted to 0.4 mm by the size of the smallest analyser aperture, and in the x direction by the diameter of the ion beam, judged to be around 0.5 mm from ion trajectory simulation. This collision volume is situated about 4 mm from the nozzle exit. Taking into account that H atoms emanate from the entire surface of the nozzle, which is about 1 mm in diameter, leads to an estimate of $90° \pm 10°$ as the range of collision angles. We assume a thermal energy distribution at 300 K for the hydrogen atoms since the nozzle is at about room temperature and the atoms may be expected to be thermalized during the transport from the discharge. Given the uncertainties in temperature and angular range with our experimental set-up, we preferred to estimate $f(v_{\rm rel})$ using the analytical formula

$$f(v_{\rm rel}) = \frac{1}{\mu\sqrt{\pi}}\left(\frac{2m_{\rm H}}{kT}\right)^{3/2}\sqrt{E(E-\bar{E}_{\rm X})}\exp\left\{-\frac{m_{\rm H}}{\mu kT}(E-\bar{E}_{\rm X})\right\}, \qquad (1)$$

where $E = E_{\rm rel} = E(v_{\rm rel}) = \frac{1}{2}\mu v_{\rm rel}^2$, $\mu = m_{\rm H}m_{\rm X}/(m_{\rm H}+m_{\rm X})$ is the reduced mass of the system and $\bar{E}_{\rm X} = \mu E_{\rm X}/m_{\rm X}$, with $E_{\rm X}$ being the laboratory ion energy. This formula is obtained from the Maxwell–Boltzmann distribution, $f_{\rm H}(v_{\rm H}) = Nv_{\rm H}^2\exp(-\frac{1}{2}m_{\rm H}v_{\rm H}^2)$, transformed into CMS velocity with the assumption of strictly perpendicular collisions, ($v_{\rm rel}^2 = v_{\rm H}^2 + v_{\rm X}^2$), and a

perfectly defined ion energy, E_X. We verified that taking the uncertainty of the collision angle, $90° \pm 10°$, and ion energy spread, $\Delta E_X = 0.4$ eV, into account does not change the resulting distribution, $f(v_{rel})$, significantly, and has only a minor influence on the electron spectra. For the interpretation of the spectra it is useful to know the mean CMS collision energy, $\langle E_{rel} \rangle$. Using the collision velocity distribution (1) we obtain

$$\langle E_{rel} \rangle = \int \frac{1}{2} \mu v^2 f(v_{rel}) \, dv_{rel} = \frac{\frac{3}{2} kT m_X + E_X m_H}{m_X + m_H}. \tag{2}$$

The difference in $\langle E_{rel} \rangle$ determined considering also the uncertainty in collision angle and ion energy is insignificant in view of the present experimental resolution.

To assess the possible influence of background atomic hydrogen, a fraction of which may possibly not recombine on the walls, we also calculated the CMS collision energy distribution for ions colliding with a stationary gas having an isotropic velocity distribution. This distribution can also be calculated analytically as

$$f_{Bg}(v_{rel}) = (\alpha - \alpha^{-1}) \left[\frac{m_H}{2\pi kT} E / \bar{E}_X \right]^{1/2} \exp\left\{ -\frac{m_H}{\mu kT} (E + \bar{E}_X) \right\}, \tag{3}$$

$$\alpha = \exp\left(\frac{2m_H}{\mu kT} \sqrt{E \bar{E}_X} \right). \tag{4}$$

The mean CMS collision energy, $\langle E_{rel} \rangle$, for this distribution is also given by the expression (2), but the distribution is much broader than that given by formula (1), because some of the H atoms now have velocities essentially parallel or antiparallel to those of the ions. This distribution does not vanish for small velocities, whereas the distribution given by expression (1) contributes only when the CMS collision energy, E_{rel}, is larger than $\bar{E}_X$. This is a particularly important property, since the cross section increases rapidly for $E \to 0$.

The background gas is expected to be nearly exclusively H_2 in the experiment. The H atoms leaving the nozzle experience on average many collisions with the vacuum chamber walls before returning to the collision region as a background gas, and H atoms recombine to H_2 very efficiently on metal surfaces. We therefore assume that all H atoms in the collision region arrive directly from the nozzle and have an essentially one-dimensional velocity distribution. The distribution of equation (1) is consequently used to calculate the theoretically predicted spectra shown in this work. We do discuss the consequences of using the distribution of equation (3) at the end of this paper, however.

2.3. Theory

We calculated the AD cross sections for the $H + Cl^-$ and $H + Br^-$ systems using the nonlocal resonance theory described in detail by Domcke (1991). The nonlocal resonance theory has been applied to calculate electron spectra due to associative detachment reaction by Čížek *et al* (2001b). The methods and potentials used here are described in detail in the papers on low energy electron scattering on these molecules (Čížek *et al* 1999, 2001a). Both experimental and theoretical work on low energy electron collisions with these two systems have been briefly reviewed by Čížek *et al* (2002).

The system is described by the three functions $V_0(R)$, $V_d(R)$ and $V_{d\varepsilon}(R)$ within the nonlocal resonance theory (figure 6). $V_0(R)$ is the standard Born–Oppenheimer potential energy for the neutral molecule HX as a function of the internuclear distance. The function $V_d(R)$ describes the temporary molecular anion HX^- (discrete state) formed during the collision and $V_{d\varepsilon}(R)$ is the coupling of the discrete state and the electronic continuum $HX + e^-$. It has been shown by Domcke (1983) that it is possible to choose the discrete state in such

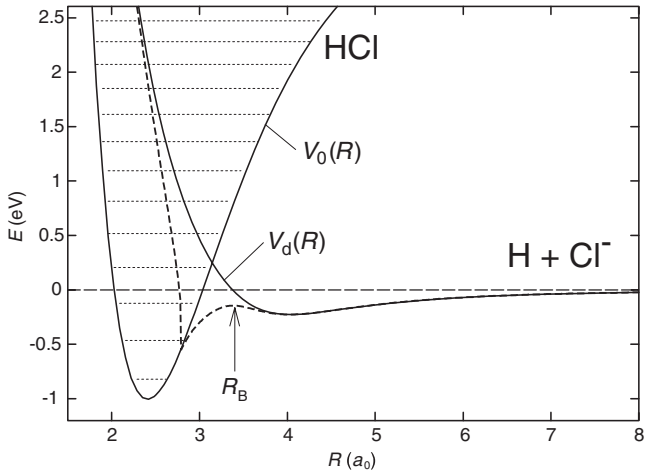

Figure 6. The potential curves of HCl and HCl^-. The dashed line indicates the energy of the bound state of HCl^-, which becomes a resonance for small R (adapted from Čížek *et al* 2001b).

a way that orthogonalization of the continuum to this state removes all singularities close to threshold from the continuum. The basis constructed in this way can be used for the description of dynamics of the system employing the Born–Oppenheimer approximation. But such a discrete state cannot be an eigenstate of the electronic Hamiltonian for small R. The discrete state potential, $V_d(R)$, thus does not describe the adiabatic energy of the bound (resonance) state, HX^-, except at large R, where the coupling to the continuum is small. The Born–Oppenheimer motion on the potential energy curve, $V_d(R)$, is thus modified due to coupling, $V_{d\varepsilon}(R)$, with the continuum, a complex energy-dependent term has to be added to $V_d(R)$ and the nuclear part of the wavefunction fulfils the equation

$$\left[-\frac{1}{2\mu}\frac{d^2}{dR^2}+\frac{J(J+1)}{2\mu R^2}+V_d(R)-E\right]\Psi_d(R) + \sum_v \chi_J^v(R)\int dR' f(\varepsilon = E - E_J^v, R, R')\chi_J^v(R')\Psi_d(R') = 0, \tag{5}$$

where $\chi_J^v(R)$ are the vibrational states in the potential $V_0(R) + J(J+1)/2\mu R^2$. The sum also includes the integral over the continuum part of the spectrum. The function f is defined as

$$f(\varepsilon, R, R') = \int d\varepsilon' \,(\varepsilon - \varepsilon' + i0)^{-1} V_{d\varepsilon'}(R) V^*_{d\varepsilon'}(R'). \tag{6}$$

Neglecting the energy dependence of the coupling amplitude, $V_{d\varepsilon}(R)$, and the assumption that the accessible vibrational states (at a given collision energy) form (approximately) a complete basis set, removes the nonlocality and the LCP method is obtained. Neither of these two approximations is correct in our case. Key to the success of the nonlocal resonance theory in the description of threshold features is retaining the dependence of the coupling amplitude $V_{d\varepsilon}(R)$ on the electron energy. For polar molecules with subcritical dipole moments like HCl and HBr, the behaviour of this quantity in the vicinity of the threshold is

$$V_{d\varepsilon}(R) \sim \varepsilon^{\alpha/2} \tag{7}$$

with $0 < \alpha < 0.5$. Such strong energy dependence causes sharp structures in the nonlocal potential (the second term in equation (5)) when the collision energies $E > E_J^v$ so that the

new channels opens. In this way inter-channel coupling between processes with the product molecule created in the final states with the same J but different v is taken into account. In contrast to the LCP method the probability flux is conserved in this method.

For the HCl and HBr systems the nonlocal resonance model (i.e., functions $V_0(R)$, $V_\mathrm{d}(R)$, $V_{\mathrm{d}\varepsilon}(R)$) has been defined fully on the basis of *ab initio* calculations (Čížek *et al* 1999, 2001a). A Morse function fitted to *ab initio* calculations and spectroscopic data is used for the potential, $V_0(R)$, of the neutral molecule. The potential $V_\mathrm{d}(R)$ and the coupling $V_{\mathrm{d}\varepsilon}(R)$ are based on eigenphases for fixed-R electron molecule scattering calculated for many values of R and ε (Padial and Norcross 1984, Fandreyer *et al* 1993). In addition, the potential $V_\mathrm{d}(R)$ is modified for large R, to take into account the calculated energies of the HX^- adiabatic state (Åstrand and Karlström 1990, Čížek *et al* 2001a). The dynamics within the nonlocal resonance model is solved, and the cross sections

$$\sigma_{v,J}(E) = \frac{2\pi^2}{E}(2J+1)|\langle\Psi_\mathrm{d}|V_{\mathrm{d}\varepsilon^v_J}|\chi^v_J\rangle|^2 \tag{8}$$

for the associative detachment process are found for all accessible ro-vibrational states, $|\chi^v_J\rangle$, with the energies $E^v_J < E$. The CMS collision energy is varied on a grid $E = 1, 2, \ldots, 500$ meV. The energy of the released electron is given by the energy conservation $\varepsilon^v_J = E - E^v_J$ and the differential cross section is

$$\frac{\mathrm{d}\sigma}{\mathrm{d}\varepsilon}(\varepsilon, E) = \sum_{J,v}\sigma_{v,J}(E)\delta(\varepsilon - E + E^v_J), \tag{9}$$

where the sum is performed over all open channels ($E^v_J < E$). For the comparison with the experiment, the CMS collision velocity distribution, $f(v_\mathrm{rel})$, has to be taken into account and the electron count rate is proportional to the reaction rate,

$$\frac{\mathrm{d}k}{\mathrm{d}\varepsilon}(\varepsilon) = \int \frac{\mathrm{d}\sigma}{\mathrm{d}\varepsilon}(\varepsilon, E(v_\mathrm{rel}))f(v_\mathrm{rel})v_\mathrm{rel}\,\mathrm{d}v_\mathrm{rel} \sim \sum_{J,v}\sigma_{v,J}(E)f(v_\mathrm{rel}(E))|_{E=\varepsilon+E^v_J}. \tag{10}$$

Here the sum is performed over those J and v for which the CMS collision energy $E = \varepsilon + E^v_J > 0$. Note that the energy scale has been chosen in such a way that the asymptotic energy of $H + X^-$ is zero, i.e., the total energy of the system, E, also gives the collision energy of $H + X^-$ in the centre of mass system.

3. Results and discussion

Figure 7 shows the experimental and theoretical results for $H + Cl^-$ collisions at 0.5 eV laboratory frame ion energy. Experiment and theory were normalized arbitrarily at low electron energies. The calculated positions of the v and S_v steps are marked. The positions of the steps were calculated using the dissociation energies $D_0(\mathrm{HCl}) = 4.434$ eV and $D_0(\mathrm{HBr}) = 3.758$ eV (Huber and Herzberg 1979) and the electron affinities $\mathrm{EA(Cl)} = 3.614$ eV and $\mathrm{EA(Br)} = 3.364$ eV (Andersen *et al* 1999, Berzinsh *et al* 1995, Blondel *et al* 1989). (The more recent value, $D_0(\mathrm{HCl}) = 4.4322$ eV, given by Martin and Hepburn (1998), is consistent with the older values.) As already pointed out by Živanov *et al* (2002), both the v and S_v steps are confirmed by the experiment. All theoretical cross sections in this paper were convoluted with a Gaussian of 30 meV width, to simulate the instrumental resolution. This choice is based on the estimate of the electron analyser resolution of 30–35 meV, as described in section 2.1. The choice seems essentially correct, in the sense that the slopes of the experimental and theoretical data around the S_1 step are consistent. The theoretical data show remnants of rotational structure which are not evident in the experimental data, however. Otherwise, there

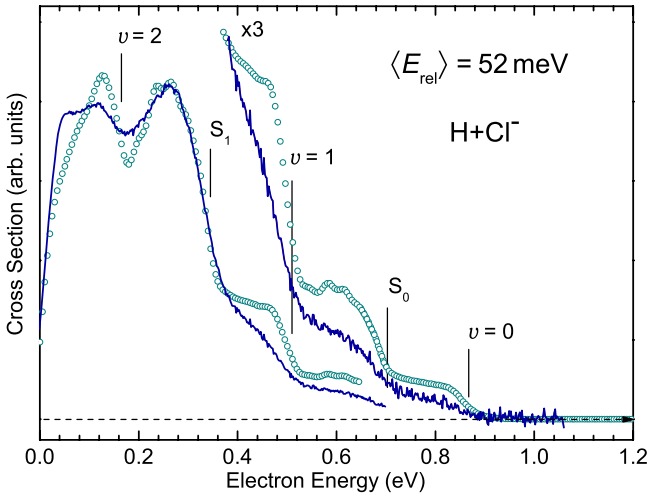

Figure 7. Experimental and theoretically predicted (circles) spectra of electrons detached in $H + Cl^-$ collisions. Laboratory frame ion energy was equal to 0.5 eV.

is a good agreement of the shapes of the theoretical and experimental curves. There are two differences in detail: the measured cross sections at higher electron energies are generally somewhat lower than the theoretical prediction, and the v steps are higher and steeper in the calculation than in the experiment.

The S steps are also clearly seen, at unchanged energies, in the spectrum recorded an laboratory frame energy of 2 eV shown in figure 8. The v steps should shift to the right by only about 40 meV, an amount comparable to the confidence limit of the energy scale, and not clearly evident. This has the consequence of closing up the valley which occurred at 0.18 eV in figure 7. The relative intensities of the signals in the 0.1–0.3 eV range, just to the left of the S_1 and $v = 2$ steps, differ somewhat in the theory and experiment. The former is larger than the latter in the experiment, the contrary is found in theory. This is consistent with the observation made already in connection with figure 7 that the v steps are generally higher and steeper in the calculation than in the experiment. The same observation is made for the $v = 1$ step in figure 8.

At the laboratory frame energy of 4 eV (figure 9), the onsets of the v steps are shifted by nearly 100 meV with respect to figure 7, and the shifts are clearly visible in both the experimental and theoretical curves. The differences between theory and experiment are the same as with the lower ion energies—the v steps are generally lower and less steep in the experiment.

With an ion energy of 8 eV, we have $\langle E_{\rm rel}\rangle = 260$ meV, the total energy with respect to the $v = 0$ level is DA + $\langle E_{\rm rel}\rangle = 1080$ meV and formation of HCl in $v = 3$ (at 1035 meV) becomes possible. Two channel closings now become relevant around the S_1 step. The $v = 3$ channel closes at low values of J (around $J = 6$) and the $v = 2$ channel closes at high values of J (around $J = 17$). The $v = 2$ onset moves, in comparison to figure 9, to the right of the S_1 step, which means that two cross sections now experience a step near the energy of S_1: that for forming HCl in $v = 1$ (at $J \approx 17$) when the $v = 2$ channel closes and a new step in the cross section for forming HCl in $v = 2$ (at $J \approx 6$) when the $v = 3$ channel closes. The latter step is labelled S_2' in figure 10. It is at nearly the same energy as S_1 and only a small distance to the left of the $v = 2$ onset (i.e., at low J), at $G(v = 3) - G(v = 2) = 332$ meV. The S_2' and

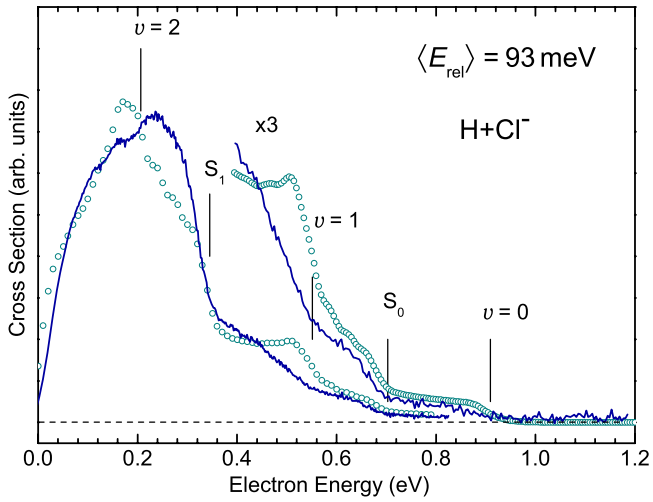

Figure 8. As figure 7, but with laboratory frame ion energy equal to 2 eV.

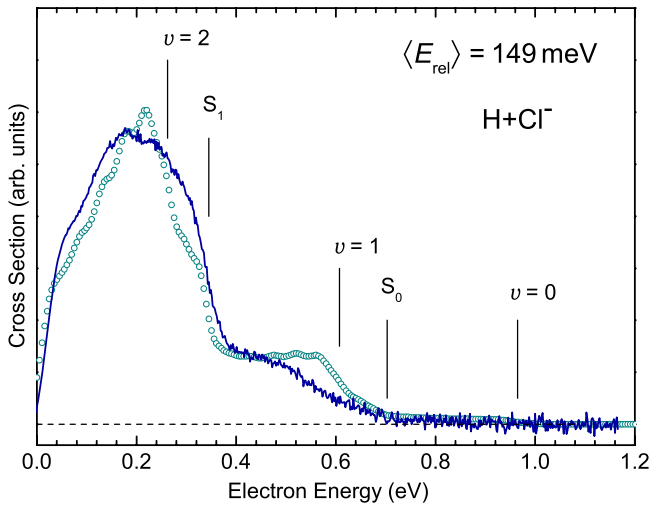

Figure 9. As figure 7, but with laboratory frame ion energy equal to 4 eV.

S_1 steps, as well as the $v = 2$ onset (at 372 meV) are close to each other, overlap at the present resolution and give rise to one high step in the experimental spectrum. There will similarly be a new step S_1', due to the effect of closing of the $v = 3$ channel on the $v = 1$ cross section. It is close to the $v = 1$ onset (i.e., at low J), at $G(v = 3) - G(v = 1) = 667$ meV. The S_1' and S_0 steps together with the $v = 1$ threshold overlap and give rise to one step in the spectra of figure 10. Note that associative detachment remains the only energetically accessible process, even at this high ion energy; the CMS energy is still well below the threshold of collisional detachment, $H + X^- \rightarrow H + X + e^-$.

Replacing hydrogen with deuterium has a trivial effect on the positions of both the v and the S steps, due to the lowering of all vibrational levels. The highest accessible vibrational level for DCl is $v = 3$ at the ion energies of 0.2 and 0.5 eV, and $v = 4$ at the ion energy of 4 eV.

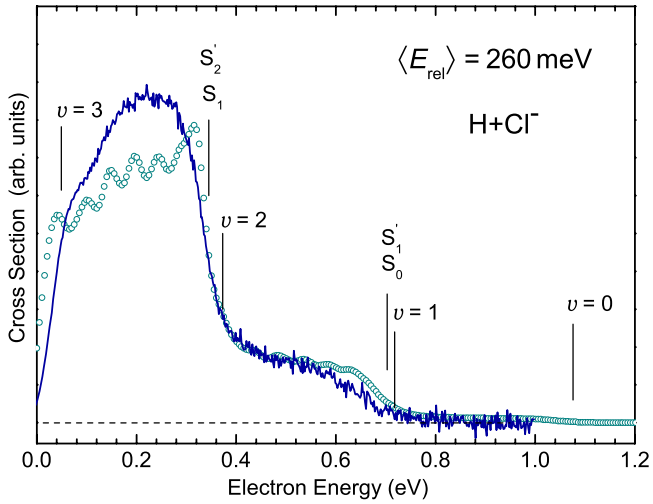

Figure 10. As figure 7, but with laboratory frame ion energy equal to 8 eV.

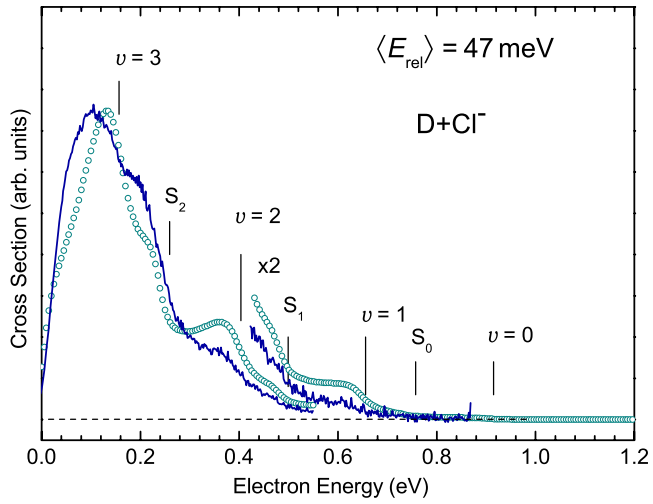

Figure 11. Spectra of electrons detached in D + Cl^- collisions at a laboratory frame ion energy of 0.2 eV.

Note that the CMS energy scale is now less 'compressed'; that is, $\langle E_{\rm rel}\rangle$ rises more rapidly with the laboratory frame energy than in the case of the lighter hydrogen isotope. The D + Cl^- spectrum in figure 11 reflects all these changes in positions of the steps, further confirming their origin. The v steps are higher and steeper in the calculation, just as in the spectra from H + Cl^- collisions. The change in the position of the v steps between figures 11 and 12 is only 16 meV, too small to be discernible with the present resolution. But the fact that the $v = 3$ step moves towards higher energies brings the $v = 3$ and the S_2 steps closer together, and has a visible effect in the spectra. The situation in figure 13 resembles that in figure 10. The collision energy has increased enough to open a new vibrational channel, $v = 4$. New steps, in particular S_3' and S_2', have appeared.

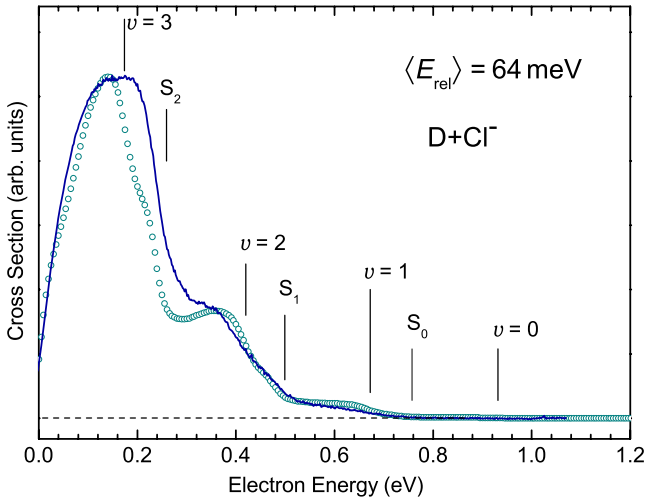

Figure 12. Spectra of electrons detached in D + Cl^- collisions at a laboratory frame ion energy of 0.5 eV.

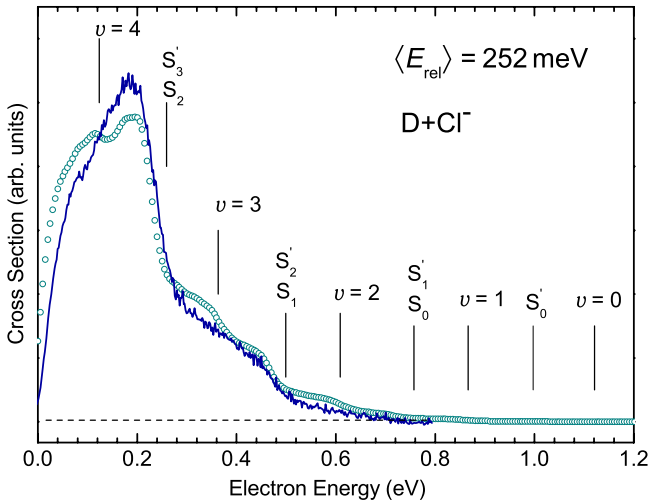

Figure 13. Spectra of electrons detached in D + Cl^- collisions at a laboratory frame ion energy of 4 eV.

The comparison of the relative heights of the steps with H and D is interesting. Whereas the signal due to formation of HCl in $v = 0$ is weak but still clearly visible in figures 7 and 8, the signal due to formation of DCl in $v = 0$ is not detectable in figure 12. Generally, the relative cross sections for the formation of low final vibrational levels are smaller with deuterium than with hydrogen. This reduction of the cross section for final states with low v can be understood qualitatively as a kinetic effect. As already discussed in the introduction, the dominance of an s wave, and consequently the absence of a rotational barrier for the departing electron, make the autodetachment rate high and lead to a 'saturation' of the detachment probability—the detachment probability along the full trajectory is essentially one. The detachment occurs mostly early in the collision, at large internuclear distances, preferring the highest available v.

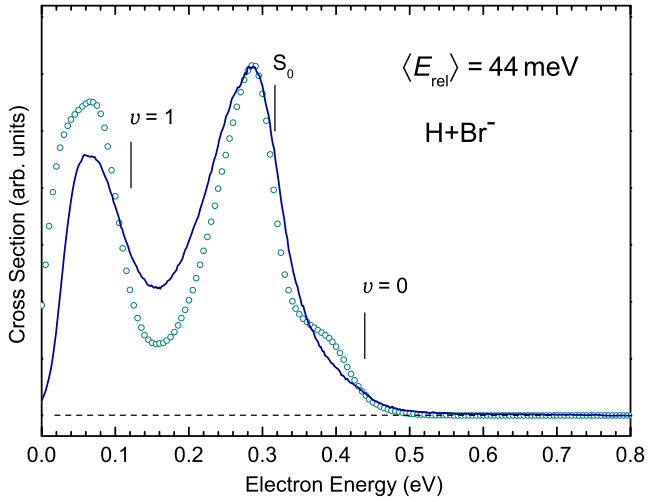

Figure 14. Electron spectra for H + Br^- collisions at a laboratory frame ion energy of 0.5 eV.

This preference is even more pronounced for the deuterium atom, which moves more slowly for the same CMS energy, leading to an even smaller probability of detachment at short internuclear distances, and hence to even lower cross sections for low final vibrational states.

The spectra resulting from H + Br^- collisions are phenomenologically similar to those already discussed, except that the highest accessible vibrational level is $v = 1$, so that only the S_0 step is present. The theoretically predicted behaviour of the two different kinds of step is confirmed by the experiment: the v steps shift to higher ϵ with increasing collision energy, while the S steps remain at constant positions.

The shift of the $v = 1$ step with increasing ion energy in figures 14–17 is manifested as a gradual closing up of the valley between the two peaks in the spectrum. As a result of this trend the valley disappears entirely in the experimental spectrum of figure 17. The v steps are generally lower and less steep in the experiment than in theory, as for the H + Cl^- collisions. The conclusions which follow from the spectra obtained with D + Br^- collisions, shown in figures 18 and 19, are similar to those obtained with isotope substitution in the case of the H + Cl^- collisions.

The data presented here show that the nonlocal resonance theory accounts essentially quantitatively for all the observations. An excellent agreement of theory and experiment is found for the shapes of the S steps. The only slight difference between the calculated and the experimental spectra, observed systematically for all collision partners and all energies studied here, is the somewhat higher and steeper v steps in the theory, more rounded steps in the experiment. This difference could be of experimental origin. Since the positions of the v steps depend, in contrast to the positions of the S steps, on collision energy, a selective broadening of the v steps as compared to the S steps could be caused by a distribution of collision energies much wider than assumed. We considered two possible causes of such broadening. An incomplete thermalization of the atomic hydrogen during its transport to the collision region would broaden the distribution, but a simulation at 400 K indicated only a small increase of the width of the v steps, insufficient to significantly improve the agreement with the experiment. We further simulated the spectra under the assumption that some or all of the atomic hydrogen has an isotropic distribution of velocities (equation (3)), that is, that it was scattered from the metal surfaces around the collision region without sticking and

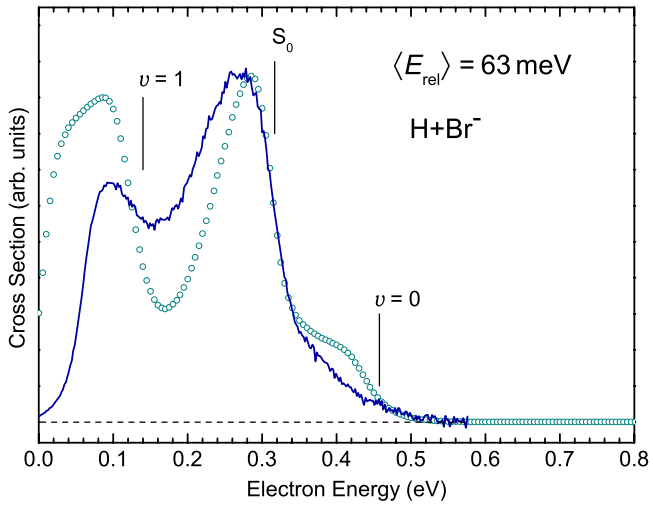

Figure 15. Electron spectra for H + Br^- collisions at a laboratory frame ion energy of to 2 eV.

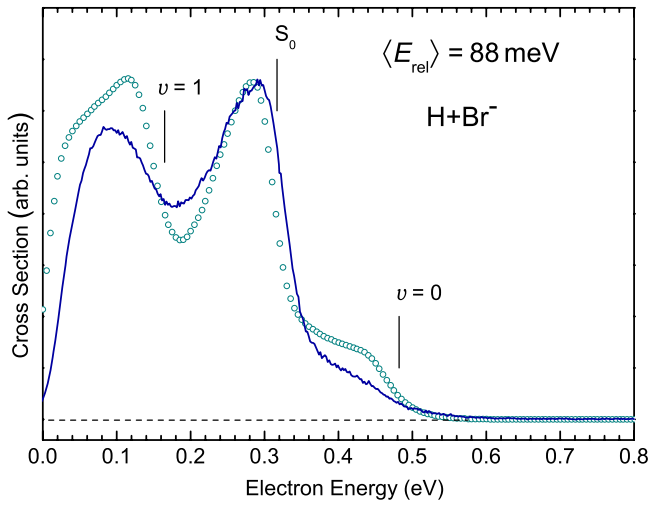

Figure 16. Electron spectra for H + Br^- collisions at a laboratory frame ion energy of 4 eV.

recombination. This assumption causes a broadening of the collision energy distribution, but the amount of the broadening depends strongly on the mean collision energy—the agreement between the calculated and the measured spectra improves only for high collision energies and the difference persists at low and intermediate collision energies (spectra calculated for the isotropic distribution have been shown by Živanov (2003)). The assumption of an isotropic velocity distribution of the H atoms is thus not a generally satisfactory explanation of the rounded v steps in the experiment.

Finally, we note that Merz *et al* (1992, 1994) found that the shape of the v steps in the related process of associative ionization, $He^*(2\,^3S) + H(1\,^2S) \rightarrow HeH^+(v, J) + e^-$, depends on the angle of detection of the ejected electron. The steps were found to be less steep at 90° than at 10° or 180°, the angular dependence being a manifestation of substantial contributions

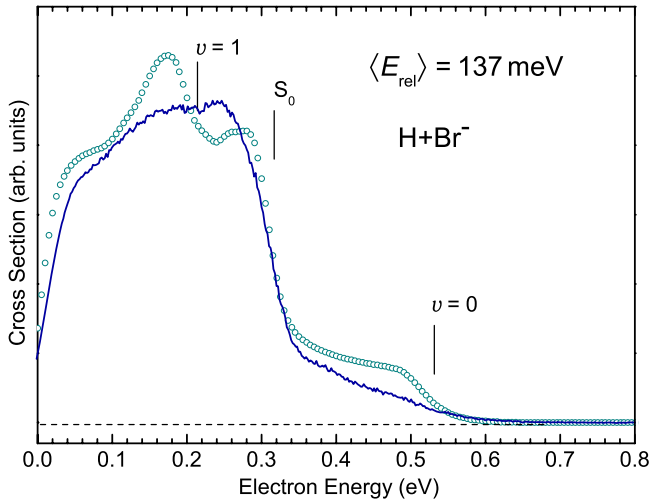

Figure 17. Electron spectra for H + Br^- collisions at a laboratory frame ion energy of 8 eV.

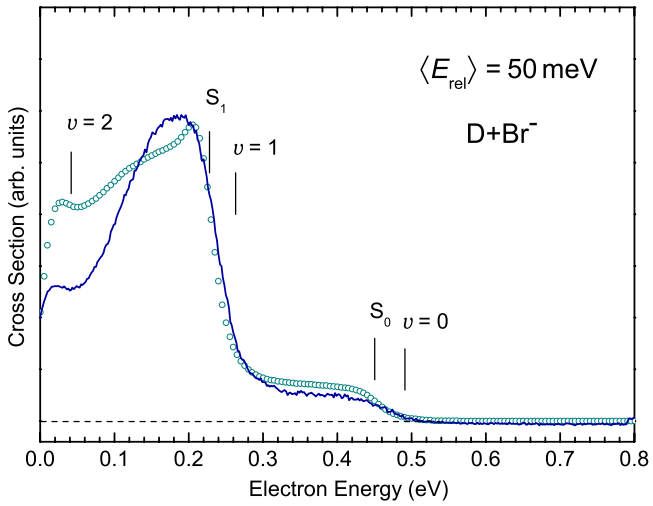

Figure 18. Electron spectra for D + Br^- collisions at a laboratory frame ion energy of 0.5 eV.

from non-s-type electron partial waves. A further study of angular dependence of the spectra and of a possible contribution of higher partial waves may thus also be needed in the present case.

4. Conclusions

The presence of both the v steps and the S steps in the experimental spectra has already been observed by Živanov *et al* (2002). The present study further confirms the origin of the two kinds of step, by showing that they behave correctly when the collision energy is varied and when the vibrational and rotational energy levels of the product molecules are shifted by isotope substitution. The cross sections for the formation of the product molecules in low vibrational levels, relative to the formation of higher vibrational levels, is smaller with deuterium than with

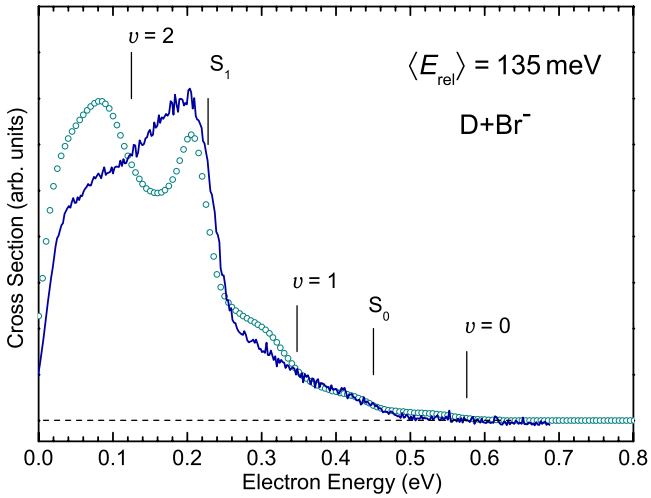

Figure 19. Electron spectra for D + Br^- collisions at a laboratory frame ion energy of 4 eV.

hydrogen. This can be understood as a consequence of the kinetics of the process. Classically speaking, the slower moving deuterium penetrates less deeply into the electronic cloud of Cl^- and Br^- before detachment occurs, leading to molecules with larger internuclear separation and hence in higher vibrational states.

The nonlocal resonance theory is shown to account essentially quantitatively for all the features of the experimental spectra. An excellent agreement of theory and experiment is found for the shapes of the S steps. The only slight difference between the calculated and the experimental spectra, observed systematically for all collision partners and all energies studied here, is the somewhat higher and steeper v steps in the theory, more rounded steps in the experiment.

Acknowledgments

This study benefitted greatly from the fruitful cooperation with F A U Thiel and H Hotop of the Kaiserslautern group in the initial stages of the work. We thank I Bray for providing theoretical cross sections for the excitation of atomic hydrogen. We also thank T Skalický for help in measuring the mass spectra of negative ions formed from CCl_4 and CBr_4 at a hot filament. MČ acknowledges support by the Grant Agency of the Czech Republic (project No GACR–203/00/D111). This research is part of project No 2000-067877.02 of the Swiss National Science Foundation.

References

Abouaf R and Teillet-Billy D 1977 *J. Phys. B: At. Mol. Phys.* **10** 2261
Allan M 1982 *Chimia* **36** 457
Allan M 1989 *J. Electron. Spectrosc.* **48** 219
Andersen T, Haugen H K and Hotop H 1999 *J. Phys. Chem. Ref. Data* **28** 1511
Asmis K R and Allan M 1997 *J. Phys. B: At. Mol. Opt. Phys.* **30** 1961
Åstrand P-O and Karlström G 1990 *Chem. Phys. Lett.* **175** 624
Berzinsh U, Gustafsson M, Hanstorp D, Klinkmuller A, Ljungblad U and Martenssonpendrill A M 1995 *Phys. Rev.* A **51** 231

Blondel C, Cacciani P, Delsart C and Trainham R 1989 *Phys. Rev.* A **40** 3698
Bray I 2001 private communication
Burrow P D 2001 private communication
Čížek M, Horáček J, Allan M and Domcke W 2002 *Czech. J. Phys.* **52** 1057
Čížek M, Horáček J, Allan M, Sergenton A C, Popović D B, Domcke W, Leininger T and Gadea F X 2001a *Phys. Rev.* A **63** 062710
Čížek M, Horáček J and Domcke W 1999 *Phys. Rev.* A **60** 2873
Čížek M, Horáček J, Thiel F A U and Hotop H 2001b *J. Phys. B: At. Mol. Opt. Phys.* **34** 983
Domcke W 1983 *Phys. Rev.* A **28** 2777
Domcke W 1991 *Phys. Rep.* **208** 97
Fandreyer R, Burke D G, Morgan L A and Gillan C J 1993 *J. Phys. B: At. Mol. Opt. Phys.* **26** 3625
Gauyacq J P 1982 *J. Phys. B: At. Mol. Phys.* **15** 2721
Gauyacq J P 1987 *Dynamics of Negative Ions* (Singapore: World Scientific)
Howard C J, Fehsenfeld F C and McFarland M 1974 *J. Chem. Phys.* **60** 5086
Huber K P and Herzberg G 1979 *Molecular Spectra and Molecular Structure* vol 4 *Constants of Diatomic Molecules* (New York: Van Nostrand-Reinhold)
Huels M A, Fedchak J A, Champion R L, Doverspike L D, Gauyacq J P and Teillet-Billy D 1994 *Phys. Rev.* A **49** 255
Martin J D D and Hepburn J W 1998 *J. Chem. Phys.* **109** 8139
Merz A, Ruf M-W and Hotop H 1992 *Phys. Rev. Lett.* **69** 3467
Merz A, Ruf M-W, Hotop H, Movre M and Meyer W 1994 *J. Phys. B: At. Mol. Opt. Phys.* **27** 4973
Padial N T and Norcross D W 1984 *Phys. Rev.* A **29** 1590
Paolini F H and Khakoo M A 1998 *Rev. Sci. Instrum.* **69** 3132
Read F H and Bowring N 2002 CPO programs http://cpo.ph.man.ac.uk
Schneider B I, LeDourneuf M and Burke P G 1979 *J. Phys. B: At. Mol. Phys.* **12** L365
Schramm A, Fabrikant I I, Weber J M, Leber E, Ruf M-W and Hotop H 1999 *J. Phys. B: At. Mol. Opt. Phys.* **32** 2153
Smith M A and Leone S R 1983 *J. Chem. Phys.* **78** 1325
Spence D and Inokuti M 1974 *J. Quant. Spectrosc. Radiat. Transfer* **14** 953
Stamatović A and Schulz G J 1968 *Rev. Sci. Instrum.* **39** 1752
Weingartshofer A, Ehrhardt H, Hermann V and Linder F 1970 *Phys. Rev.* A **2** 294
Živanov S 2003 *PhD Thesis* University of Fribourg
Živanov S, Allan M, Čížek M, Horáček J, Thiel F A U and Hotop H 2002 *Phys. Rev. Lett.* **89** 073201
Zwier T S, Maricq M M, Simpson C J S M, Bierbaum V M, Ellison G B and Leone S R 1980 *Phys. Rev. Lett.* **44** 1050